e-ISSN 2083–4640
ISSN 1507–1367

RESEARCH PAPER

Reports of Practical Oncology and Radiotherapy
2022, Volume 27, Number 5, pages: 809–820
DOI: 10.5603/RPOR.a2022.0089
Submitted: 02.07.2022
Accepted: 12.08.2022

Setup accuracy and dose attenuation of a wooden immobilization system for lung stereotactic body radiotherapy

Yuya Nitta[1], Yoshihiro Ueda[1], Seiya Murata[1], Masaru Isono[1], Shingo Ohira[1], Akira Masaoka[1], Shoki Inui[1, 2], Hayate Washio[3, 4], Reimi Yoshinaka[1], Tomohiro Sagawa[1], Masayoshi Miyazaki[1], Teruki Teshima[5]

[1]Department of Radiation Oncology, Osaka International Cancer Institute, Osaka, Japan
[2]Department of Medical Physics and Engineering, Osaka University Graduate School, Osaka, Japan
[3]Department of Radiology, Osaka International Cancer Institute, Osaka, Japan
[4]Graduate School of Health Sciences, Kumamoto University, Kumamoto, Japan
[5]Osaka Heavy Ion Therapy Center, Osaka, Japan

ABSTRACT

Background: We evaluated the setup error and dose absorption of an immobilization system with a shell and wooden baseplate (SW) for lung stereotactic body radiotherapy (SBRT).

Materials and methods: Setup errors in 109 patients immobilized with an SW or BodyFix system (BF) were compared. Dose attenuation rates of materials for baseplates were measured with an ion-chamber. Ionization measurements were performed from 90° to 180° gantry angle in 10° increments, with the ball water equivalent phantom placed at the center of the wood and carbon baseplates whose effects on dose distribution were compared using an electron portal imaging device.

Results: The ratio for the anterior-posterior, cranial-caudal, and right-left of the cases within 3-mm registered shifts in interfractional setup error were 90.9%, 89.2%, and 97.4% for the SW, and 93.2%, 91.6%, and 98.0% for the BF, respectively. For intrafractional setup error, 98.3%, 97.4%, and 99.1% for the SW and 96.6%, 95.8%, and 98.7% for the BF were within 3-mm registered shifts, respectively. In the center position, the average (minimum/maximum) dose attenuation rates from 90° to 180° for the wooden and carbon baseplates were 0.5 (0.1/2.8)% and 1.0 (–0.1/10.1)% with 6 MV, respectively. The gamma passing rates of 2%/2 mm for the wooden and carbon baseplates were 99.7% and 98.3% ($p < 0.01$).

Conclusions: The immobilization system with an SW is effective for lung SBRT since it is comparable to the BF in setup accuracy. Moreover, the wooden baseplate had lower radiation attenuation rates and affected the dose distribution less than the carbon baseplate.

Key words: lung SBRT; wooden baseplate; setup verification

Rep Pract Oncol Radiother 2022;27(5):809–820

Introduction

Stereotactic body radiation therapy (SBRT) is a standard treatment modality for early-stage lung cancer [1–6]. The requirements for SBRT are generally a few treatment fractions with a high-dose in each treatment. The high-dose area is confined to the target, and it shrinks rapidly outside the target

Address for correspondence: Yoshihiro Ueda, Department of Radiation Oncology, Osaka International Cancer Institute, 3-1-69 Otemae, Chuo-ku, Osaka 537–8567, Japan; e-mail: ueda-yo@mc.pref.osaka.jp

area to spare the surrounding organs. Therefore, SBRT for lung requires accurate localization of the tumor [4–8].

Cone-beam computed tomography (CBCT), which provides volumetric images of patient anatomy, improves setup reproducibility and reliability of the patient treatment position [9–12]. Therefore, CBCT is commonly used in SBRT for lung cancer. However, the internal motion of lung tumors cannot be ignored even when the bony anatomy is matched [2]. Given the high-doses and steep dose gradients required for lung SBRT, the effects of inter- and intrafractional motion of lung tumors are clinically significant [10, 13].

Various types of immobilization systems have been developed to reduce the inter- and intrafractional motion of lung tumors. The Elekta body frame (Elekta, Stockholm, Sweden) and the BodyFix system (BF: Elekta, Stockholm, Sweden) have commonly been used. Furthermore, the Prolock (Civco Medical Solutions, Coralville, Iowa, USA) combines an abdominal compression plate with vacuum immobilization, and an immobilization system with a body shell has also been used [14–17]. Since inter- and intrafractional motion of lung tumor depends on the immobilization system, new immobilization systems for lung SBRT need to be evaluated. Moreover, immobilization systems are often connected to the top of the couch using a baseplate or similar device [18]. Baseplate devices are made from carbon fiber and polymethyl methacrylate. They attenuate the radiation dose and increase the skin dose depending on their material and thickness [18–20].

A new immobilization system was developed by combining a wooden baseplate with a body shell. To evaluate the effectiveness of this immobilization system, the setup errors and time were compared with those of the BF. Furthermore, the effect of dose absorption in the wooden baseplate, the material used in the new immobilization system, was compared with the carbon baseplate.

Materials and methods

Patient's characteristics

In total, 109 patients treated with SBRT for primary cancer or metastases in the lung between April 2017 and January 2020 were included. Initially, the BF was used for 58 patients who received lung SBRT. Subsequently, 51 patients were immobilized using an immobilization system with a shell and wooden baseplate (SW; AirFix system, Engineering System, Nagano, Japan). Two patients received 50 Gy in five fractions, and the other patients received 48 Gy in four fractions. The Ethics Committee of OICI approved the study (review board number: 20251).

The patient and tumor characteristics are summarized in supplementary material. The patient characteristics collected included age, sex, performance status using the Eastern Cooperative Oncology Group scale, and tumor characteristics, including tumor size and location.

Immobilization system

Figures 1A and B show the SW during computed tomography (CT) simulation and treatment with SBRT. The SW consisted of a vacuum cushion, thermoplastic sheet, balloon, and a wooden baseplate. The balloon was placed on each patient's abdomen, and the thermoplastic sheet was used as a cover. The balloon was inflated by injecting air, which compressed the patient's abdomen, and forced shallow breathing. The amount of air to inject into the balloon was considered the maximum volume tolerated by each patient. The cost of the SW was approximately 7,000 US dollars.

The wooden baseplate was constructed of oak wood, which is sufficiently dry, and minimally deformed. When the side plates of the wooden baseplate were pulled upward at 100 N with the center of the wooden baseplate fixed, the wooden baseplate was designed to be within about 1 mm of deformation. Furthermore, it was recommended that the wooden baseplate be wiped with a soft cloth moistened with ethanol or isopropanol in the case of heavy soiling.

Figures 1C and D show the BF during computed tomography (CT) simulation and treatment with SBRT. The BF was composed of a vacuum cushion, a clear cover sheet, a cushion for abdominal compression, and a vacuum pump. The patient was covered with a clear cover sheet, and a cushion for abdominal compression was placed on the patient's abdomen. When the vacuum pump sucked in air, the clear cover sheet and abdominal compression cushion exerted downward pressure on the abdomen, and the patient was immobilized and forced to limit their

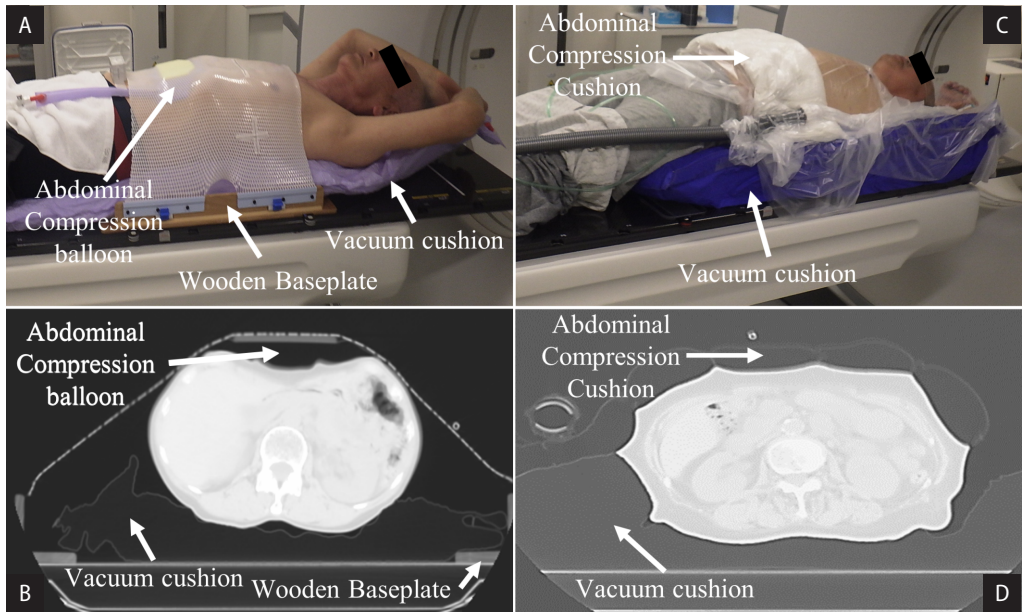

Figure 1. The two immobilization systems showing the abdominal compression cushion/balloon. The immobilization system with a shell and a wooden baseplate (SW) and the BodyFix system (BF) are shown in (**A**) and (**C**). Computed tomography images of the SW and BF are shown in (**B**) and (**D**)

breaths. The cost of the BF was approximately 160,000 US dollars.

Simulation and treatment planning

A Revolution HD CT scanner (GE Medical Systems, Waukesha, WI, USA) was used to acquire the images for planning. The parameters for image acquisition were 2.5-mm slice thickness, 512 × 512 matrix, and 500-mm field of view (FOV). All patients underwent four-dimensional CT with free-breathing, and their respiratory waveforms were recorded using a real-time position management system (Varian Medical Systems, Palo Alto, CA, USA). Average intensity projection (AIP) and maximum intensity projection (MIP) images were generated from ten respiratory-phase images.

The planning target volume (PTV) and normal tissue were delineated on AIP using the Eclipse treatment planning system (TPS; Varian Medical Systems, Palo Alto, CA, USA) by radiation oncologists at the Osaka International Cancer Institute. The PTV was defined as the area with a 5-mm margin in the internal target volume (ITV). The ITV was generated using the MIP reconstructed from the ten-phase images. If the tumor moved more than 1 cm in a longitudinal direction, a 6–8-mm longitudinal margin was added around the ITV.

SBRT treatment was performed with a Varian Truebeam STx and Varian Truebeam Edge (Varian Medical Systems, Palo Alto, CA, USA) linear accelerators. All treatment planning was performed using a volumetric modulated arc therapy (VMAT) plan with 6 MV and 6 MV flattening filter-free photons (FFF). The VMAT plans included 3-5 coplanar arcs to deliver 48-50 Gy in four to five fractions. Dose calculation was performed with a 2.0-mm grid size using the Anisotropic Analytical Algorithm ver. 15.6 (Varian Medical Systems, Palo Alto, CA, USA).

Image guidance and data collection for setup efficacy

Through a two-step online CBCT based image matching process, patients on Perfect pitch couch (Varian Medical Systems, Palo Alto, CA, USA) underwent image-guided radiation therapy. The CBCT images were acquired at 125 kVp, 80 mA, and 13 ms with a gantry rotation of 360° and were reconstructed with a slice thickness of 1 mm.

Setup time was measured to evaluate the efficiency of the SW and BF. Setup time was defined as the time from opening to closing the clinical treatment plan minus the time for image matching and irradiation and was recorded for each fraction.

Data collection for the setup accuracy was conducted as follows. First, an initial CBCT was acquired before each treatment session. On the initial CBCT, image alignment was performed using the bony anatomy before lung tumor registration. Subsequently, registration of the ITV contour was performed to the lung tumor, and couch shifts were applied. The differences between the couch shift of the tumor matching and bone matching in the initial CBCT were recorded as interfractional setup errors. A second CBCT was then acquired before irradiation of the final beam, and the couch shifts of the second CBCT were performed after correcting the setup errors. Displacements on the second CBCT scan, which were intrafractional setup errors, were recorded.

The displacements were quantified in both translational and rotational directions to evaluate the inter- and intrafractional setup errors. The translational direction was defined as anterior-posterior (AP), cranial-caudal (CC), and right-left (RL). The rotational directions represent rotations around each patient's left-right axis (pitch), CC axis (roll), and AP axis (yaw).

To compare the accuracy of the setup error between the immobilization systems, the group mean, systematic and random errors were calculated. The group mean values were defined as the average of individual values of all treatment fractions from all patients. Systematic and random errors were defined as the standard deviation (SD) of the average interpatient variability, and the root mean square of the individual SDs, respectively. The three-dimensional vector was calculated from the translational axes using the formula $(AP^2 + CC^2 + LR^2)^{0.5}$.

Radiation dose attenuation for baseplates

Figures 2A and B show the wooden and carbon baseplates (MTPLVC04MR, CIVCO Medical Solutions, Coralville, IA, USA), and Figures 2C and D show the geometry of measurements in the upper and center positions. For assessing the dose absorption of the baseplates, the dose attenuation was measured with a CC13 (IBA Dosimetry, Schwarzenbruck, Germany) ionization chamber, with the ball phantom (Taisei Medical Co., Ltd, Osaka, Japan) placed at its center of 20-cm diameter, made by water-equivalent solid phantom (Solid Water HE, Gammex Inc, Wisconsin, USA). The ball phantom was placed at the upper and center positions of the wooden and carbon baseplates, respectively. The ball phantom setup was aligned using CBCT.

The irradiation settings included nominal energy of 6 MV and 6 FFF X-ray beams with a field size of 5×5 cm^2 at 100 Monitor unit values. Ionization measurements were performed by irradiating three times from 90° to 180° gantry angles, in 10° increments, and the average value for each angle was calculated. The measurement was divided down into three zones. Zone 1 was between 90° and 100° where the baseplates were not included in the irradiation field. Zone 2 was an angle between 100° and 130° where the baseplates in the upper and center positions were included in the irradiation field. Zone 3 was an angle of 130° to 180° where baseplates in only the upper position were included in the irradiation field.

The relative attenuation dose rate was calculated using the dose irradiated under the same conditions with the treatment couch only as reference. The attenuation dose rate was defined as eq. (1)

$$Attenuation\ Dose\ Rate\ (\%) = \frac{(D_c - D_{cb}) \times 100}{D_c} \quad (1)$$

where D_{cb} represents the dose measured with the beam passing through the treatment couch and baseplate and D_c represents the dose measured with the beam passing through only the treatment couch.

Effect of dose absorption for baseplates on dose distribution

The effects of dose absorption for the wooden and carbon baseplates on dose distributions were compared using an electronic portal imaging device (EPID, Varian Medical Systems, Palo Alto, CA, USA). The measurement arrangements and the dose distributions for irradiating the anthropomorphic phantom (PH-47, Kyoto Kagaku, Kyoto, Japan) without the baseplate as reference images, and with the wooden and carbon baseplates are shown in Figure 3.

The dose distribution of the clinical treatment plan was acquired using the integrated dose image acquisition mode of amorphous silicon EPID (aS-1200), with an active area of 400 mm × 400 mm and a pixel size of 0.34 mm. For the clinical treatment plans, 10 plans were selected from the lung

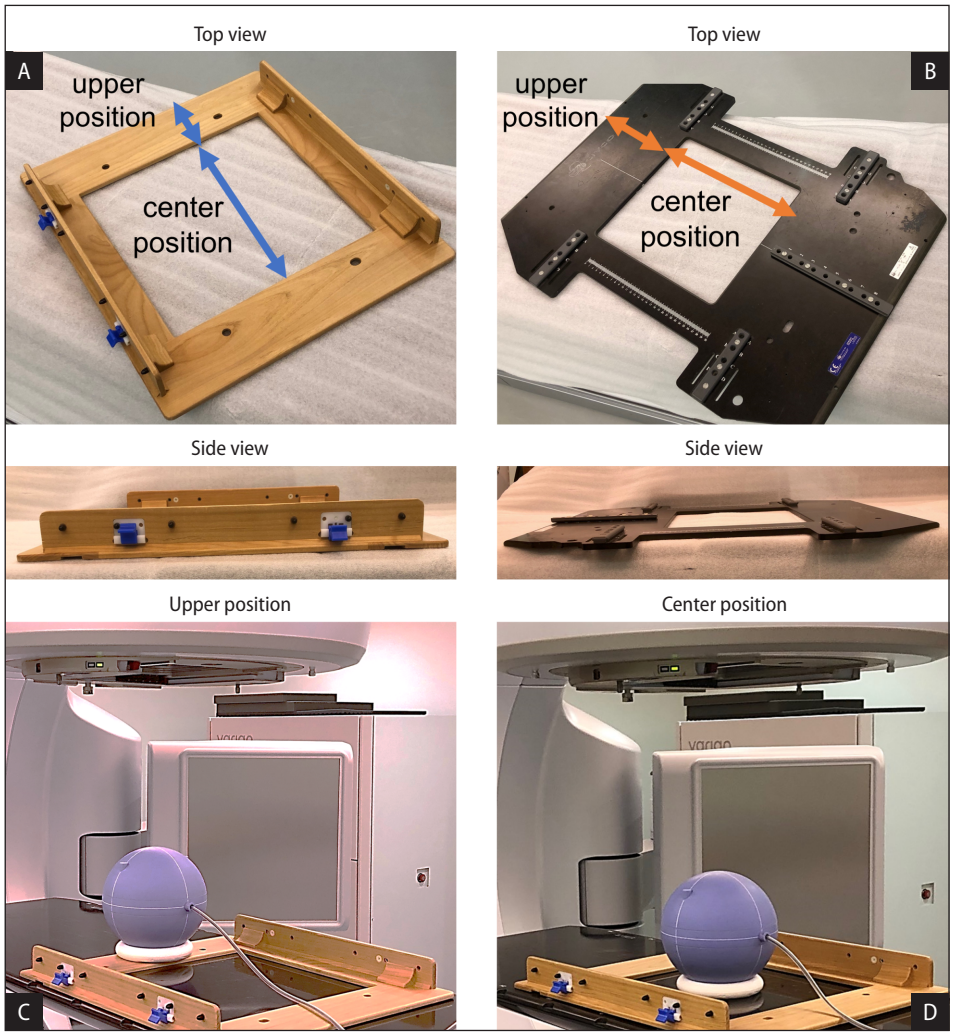

Figure 2. Measurement geometry of the dose attenuation rate for baseplates. The wooden and carbon baseplates are shown in (**A**) and (**B**), respectively. The measurement geometry in upper and center positions are shown in (**C**) and (**D**), respectively

SBRT treatment plans in which all arcs included a gantry angle of 90° to 180°. The clinical treatment plans were calculated with CT images including the anthropomorphic phantom and treatment couch.

The procedure of this study is detailed below. First, the integrated dose images as reference images were obtained by irradiating the anthropomorphic phantom without the baseplate. Next, the respective integrated dose images irradiated to the anthropomorphic phantom immobilized with the wooden and carbon baseplates were acquired. The anthropomorphic phantom was immobilized in the upper and center positions, respectively. For all cases, CBCT was performed before irradiation and matched with the anthropomorphic phantom in translation and rotation shift.

Using commercially available dosimetry software (PerFRACTION version 2.0.4, Sun Nuclear Corporation, Melbourne, FL), 10 cases were analyzed for the integrated dose images, respectively with the wooden and carbon baseplates. All integrated dose images were normalized to the maximum dose. The gamma passing rate, dose difference, and dose difference at the center point were calculated for each beam, and the average of one case was defined as the result. The criteria for the gamma passing rate and dose difference were set at 3%/3 mm, 2%/2 mm, and 1%/1 mm, and 10%, 7%, 5%, and 3%, respectively. The gamma passing rate and dose difference were defined as the percentage of points for areas exposed to more than 10% of the maximum dose. The difference in dose at the center point of the PTV between the integrated

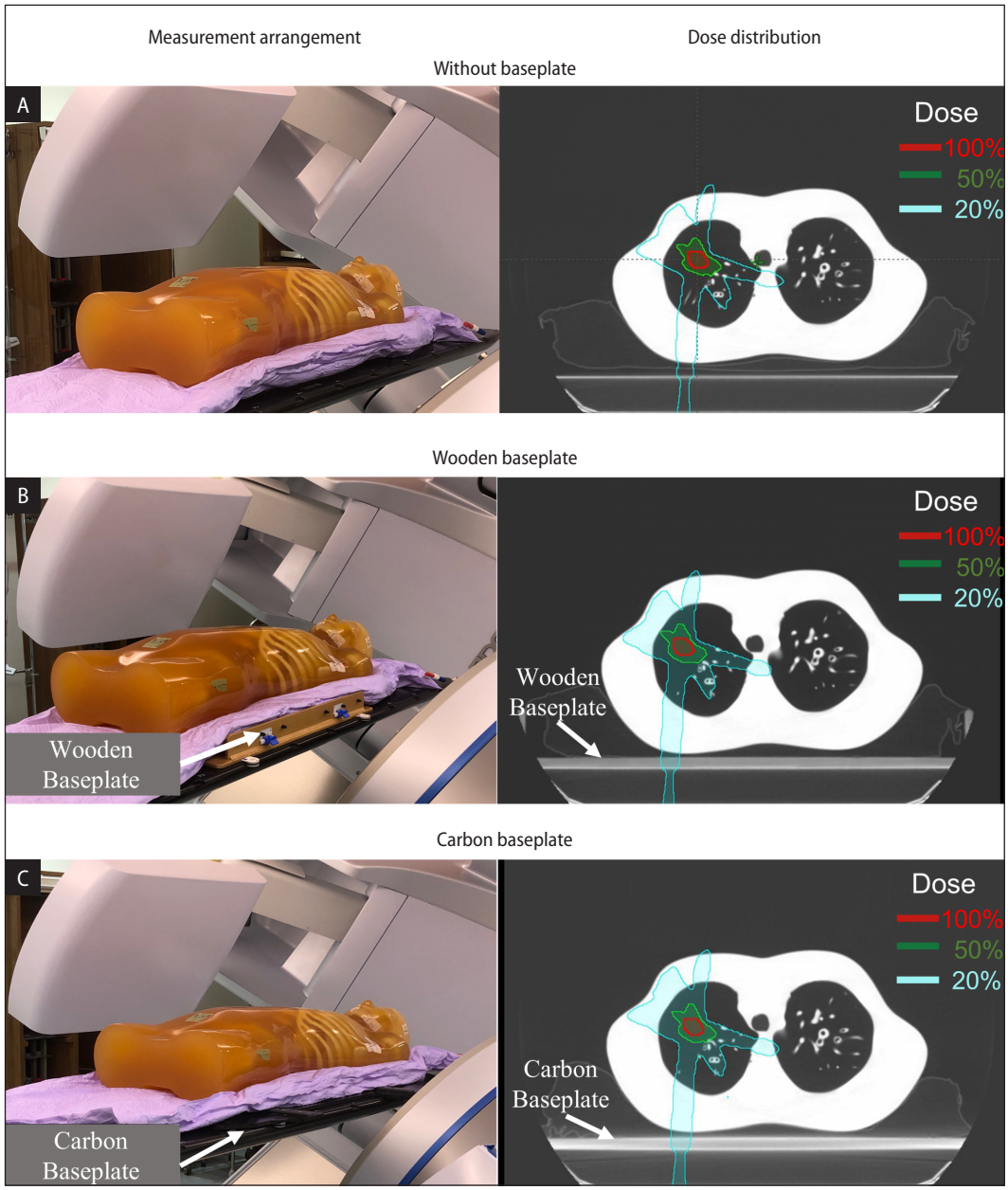

Figure 3. Measurement arrangements acquired integrated dose images and dose distributions without a baseplate and with wooden and carbon baseplates. The anthropomorphic phantom without a baseplate as reference images, immobilized with the immobilization device with a wooden baseplate, and immobilized with a carbon baseplate are shown in (**A**), (**B**), and (**C**), respectively

dose image of the reference and the integrated dose image with the wooden or carbon baseplates was defined as the dose difference at the center point.

Statistical analysis

To compare the setup time and setup error between the immobilization systems, the Mann Whitney's U test was performed. A paired Wilcoxon signed-rank test was used to determine the difference in the effect of dose absorption on the dose distribution between immobilization systems. All statistical analyses were performed using SPSS (version 25; SPSS Inc., Chicago, IL, USA). All reported p-values were two-sided with a significance level of 0.05.

Results

Setup time

The median (minimum/maximum) setup time required for the SW was significantly reduced

Table 1. Group mean values and systematic and random errors for interfractional setup error of a shell and wooden baseplate and BodyFix immobilization systems

		SW			BF			p-value
		Group mean	Σ	σ	Group mean	Σ	Σ	Group mean
Inter fractional setup error	AP [mm]	0.2	1.6	1.3	–0.7	1.5	1.2	<0.05
	CC [mm]	–0.6	1.8	1.5	–0.2	1.4	1.5	0.364
	RL [mm]	0.0	0.9	0.8	0.0	1.0	0.9	0.976
	Pitch (°)	0.2	0.5	0.9	0.1	0.7	0.6	0.327
	Roll (°)	0.0	0.4	0.5	–0.1	0.7	0.7	0.872
	Yaw (°)	0.0	0.3	0.4	0.1	0.6	0.6	0.190
	3D [mm]	2.1	1.6	1.7	2.0	1.4	1.7	0.915

SW — immobilization system with a shell and wooden baseplate; BF — BodyFix system; AP — anterior-posterior; CC — cranial-caudal; LR — left-right; pitch — patient's left-right axis; roll — patients cranial-caudal axis; yaw — patients anterior-posterior axis; Σ — systematic error; σ — random error

($p < 0.01$) compared to the BF: 450 (231/1021) and 834 (466/2336) seconds, respectively.

Interfractional setup error

The group means and the systematic and random values for the interfractional setup errors are summarized in Table 1. The group means for the SW and BF indicated similar trends, except in the AP direction, where the difference was significant ($p < 0.05$). In the SW, the group mean shifted to the anterior side on the AP axis and posterior side in the BF. The systematic translation error of SW was larger than that of BF in the CC direction and was comparable in the other directions. The results of random errors for the SW and BF were not different for any translational direction. For rotational setup error, the group means of the registered shifts for the SW and BF were not significantly different. Except for random errors in pitch, the systematic and random errors in the rotational direction for the SW were smaller than those for the BF.

Figure 4A presents the frequencies within the translational tolerances of the interfractional setup error for the SW and BF. The ratios of AP, CC, and RL for the cases within registered shifts of 3 mm were 90.9%, 89.2%, 97.4% for the SW, and 93.2%, 91.6%, and 98.0% for the BF. For the cases within registered shifts of 5 mm, they were 97.4%, 94.4%, 99.6%, and 98.7%, 98.0%, and 99.6% for the SW and BF, respectively.

Intrafractional setup error

Table 2 summarizes the group means and the systematic and random values for intrafractional setup errors. The group means of the registered shifts for the SW and BF in the translation and rotation directions were not significantly different, except for the pitch, where the difference was significant ($p < 0.01$). Systematic errors for the SW in the AP direction were larger than those for the SW. However, the other systematic and random errors for the SW were smaller than those for the BF. For rotational directions, systematic and random errors for the SW were smaller than those for the BF.

Figure 4B represents the frequencies within the translational tolerances of the intrafractional setup error for the SW and BF. For the AP, CC, and RL ratios, 98.3%, 97.4%, and 99.1%, and 96.6%, 95.8%, 98.7% were within registered shifts of 3 mm for the SW and BF, respectively. Similarly, 99.6%, 100%, 100%, and 99.6%, 99.6%, and 99.6% were within registered shifts of 5 mm for the SW and BF, respectively.

Dose attenuation rate for baseplates

The relationships between the measured gantry angle and dose attenuation rates are shown in Figure 5, where (A) and (B) indicate upper and center positions, respectively. In the upper position, the average (minimum/maximum) dose attenuation rates with 6 MV and 6 FFF were 1.9 (0.1/4.0)% and 2.3 (0.2/4.5)% for the wooden baseplate and 4.6 (-0.1/10.2)% and 5.4 (0.2/11.5)% for the carbon baseplate, respectively. In the center position, the average attenuation rates with 6 MV and 6 FFF were 0.5 (0.1/2.8)% and 0.6 (0.1/3.1)% for the wooden baseplate, and 1.0 (–0.1/10.1)% and 1.1 (–0.1/11.1)% for the carbon baseplate, respectively.

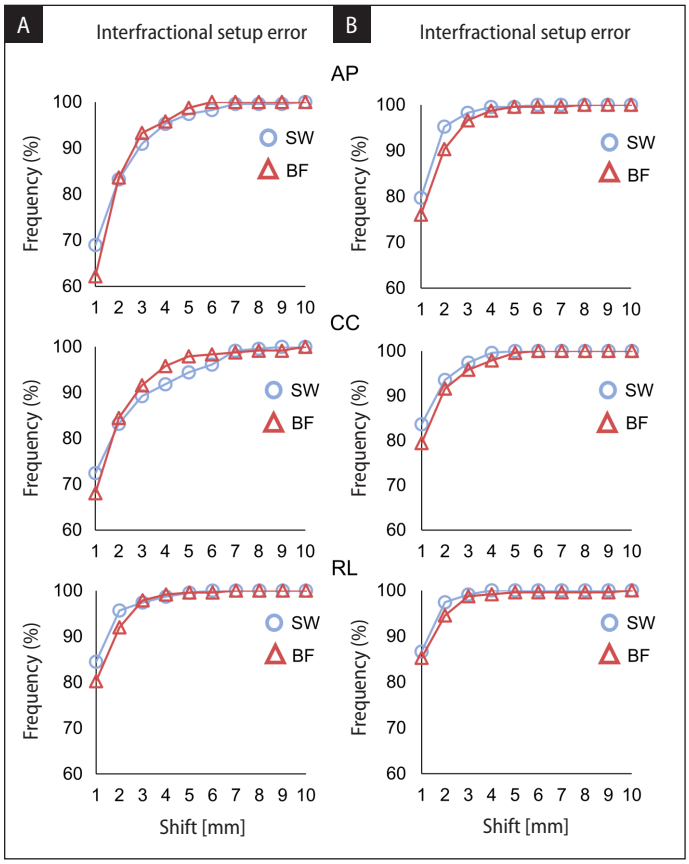

Figure 4. Graphs of the frequencies within the translational tolerances of the setup error for immobilization system with a shell and a wooden baseplate (SW) and the BodyFix system (BF). The inter and intrafractional setup errors are shown in (**A**) and (**B**). The top, middle, and bottom images represent the anterior-posterior (AP), cranial-caudal (CC), and left-right (LR) directions, respectively. The blue circle and red triangle represent the SW and BF, respectively

Table 2. Group mean values and systematic and random errors for intrafractional setup error of a shell and wooden baseplate and BodyFix immobilization systems

		SW			BF			p-value
		Group mean	Σ	σ	Group mean	Σ	σ	Group mean
Intra fractional setup error	AP [mm]	–0.7	1.0	0.8	–0.8	0.9	1.0	0.722
	CC [mm]	–0.2	0.7	1.0	–0.1	0.9	1.1	0.403
	RL [mm]	–0.1	0.7	0.7	–0.1	0.9	1.0	0.464
	Pitch (°)	–0.1	0.2	0.3	0.1	0.3	0.5	< 0.01
	Roll (°)	–0.1	0.3	0.3	–0.2	0.5	0.5	0.827
	Yaw (°)	0.0	0.2	0.2	0.0	0.3	0.4	0.842
	3D [mm]	1.3	0.9	1.3	1.5	1.1	1.6	0.412

SW — immobilization system with a shell and wooden baseplate; BF — BodyFix system; AP — anterior-posterior; CC — cranial-caudal; LR — left-right; pitch — patient's left-right axis; roll — patients cranial-caudal axis; yaw — patients anterior-posterior axis; Σ — systematic error; σ — random error

Effect of dose absorption for baseplates on dose distribution

Table 3 summarizes the gamma passing rate, dose difference, and dose difference at the center point for integrated dose images for the wooden and carbon baseplates. For all analysis parameters, except 10%, 7%, and 5% of the dose difference in the center position, the wooden baseplate had significantly less effect on the dose distribution than the carbon baseplate ($p < 0.01$).

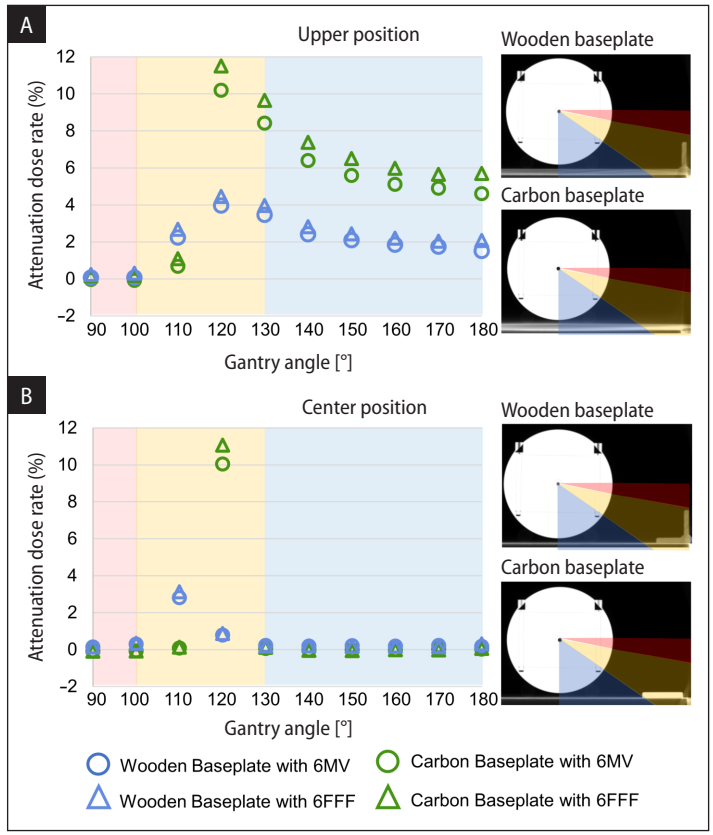

Figure 5. Relationships between the measured gantry angle and dose attenuation rates. The dose attenuation rates in the upper and center positions are shown in (**A**) and (**B**) respectively. Zone 1 is indicated by red, Zone 2 by yellow, and Zone 3 by blue. The blue circle and triangle represent the wooden baseplate with 6 MV and 6 MV flattening filter-free photons (FFF), respectively. The green circle and triangle indicate the carbon baseplate with 6 MV and 6 FFF, respectively

Table 3. Gamma passing rate, dose difference, and dose difference at the center point for integrated dose images for a shell and wooden and carbon baseplates

		Upper position			Center position		
		Wooden baseplate	Carbon baseplate	p-value	Wooden baseplate	Carbon baseplate	p-value
Gamma passing rate (%)	3%/3 mm	99.9 ± 0.1	95.4 ± 2.4	< 0.01	100.0 ± 0.0	99.9 ± 0.2	< 0.01
	2%/2 mm	99.1 ± 1.8	87.1 ± 4.0	< 0.01	99.7 ± 0.2	98.3 ± 1.2	< 0.01
	1%/1 mm	95.0 ± 7.3	66.8 ± 4.7	< 0.01	93.1 ± 3.1	90.8 ± 5.4	< 0.01
Dose difference (%)	10%	100.0 ± 0.0	99.6 ± 0.7	< 0.01	100.0 ± 0.0	100.0 ± 0.0	0.32
	7%	100.0 ± 0.0	74.4 ± 9.4	< 0.01	100.0 ± 0.1	99.9 ± 0.3	0.29
	5%	97.6 ± 4.8	51.1 ± 6.9	< 0.01	99.7 ± 0.6	98.5 ± 1.8	0.038
	3%	90.2 ± 18.7	36.9 ± 21.3	< 0.01	89.6 ± 7.4	68.0 ± 14.7	< 0.01
Dose difference at the center point (%)	–	2.1 ± 1.6	7.5 ± 1.2	< 0.01	2.1 ± 1.6	3.0 ± 1.3	< 0.01

Discussion

This study compared the inter- and intrafractional setup errors of the SW and BF in 109 patients who underwent lung SBRT. To the best of our knowledge this is the first evaluation of the SW setup accuracy, while there are many reports on the setup accuracy of the BF [16, 21–23]. As the SW is a new immobilization system, the setup time and accuracy were compared to traditional im-

mobilization systems such as the BF. Furthermore, the dose attenuation and the effect on dose distribution for wooden and carbon baseplates were evaluated. In recent years, the use of VMAT, which is a rotational type of irradiation technique, has been increasing, and it is difficult to avoid the effects of X-ray attenuation and scattering by materials in the patient's surroundings [24]. Therefore, it is important to evaluate the effect of materials in the patient's surroundings on dose distribution.

The SW required less labor for patient immobilization and abdominal compression compared to the BF; therefore, the setup time was reduced compared to the BF. More than 25 minutes of patient's remaining on the treatment couch was reported to increase intrafractional setup error [25]. The SW has an advantage compared to the BF by reducing intrafractional setup error in SBRT, which required more time to deliver higher dose than conventional treatments.

Regarding interfractional setup error, there was a statistically significant difference in group mean in the AP direction between the SW and BF. In abdominal compression systems, such as the SW, which compress the abdomen from the anterior side only, it was reported that the tumor position was displaced in the AP direction for interfractional setup errors [15, 26, 27]. Since the diaphragm movement is restricted by the abdominal compression system, the anterior shift in the tumor location is due to increased chest wall breathing. However, Strydhorst et al. reported that a thermoplastic sheet restricted chest motion in AP directions [28]. Therefore, interfractional setup error of the SW was 0.2 mm in the anterior direction. On the other hand, Foster et al. detected interfractional setup errors in the posterior direction due to the patient's body moving downward due to small leakage in the vacuum cushion and relaxation effect [29]. The setup error of the BF was 0.7 mm in the posterior direction due to the longer setup time for the BF compared to the SW, which increased the effect of relaxation and small leakage of the vacuum cushion. Although both SW and BF shifted less than 1 mm in the AP direction, SW and BF were significantly different due to the opposite direction of shift.

Several papers have reported the effectiveness of tumor matching [30–32]. In this study, for the intrafractional setup error, the systematic error of translocation for the SW ranged from 0.7 to 1.0 mm and was 0.9 mm for the BF, and the random error ranged from 0.7 to 1.0 mm, and 1.0 to 1.1 mm, respectively. For the rotational direction, the systematic error for the SW and BF ranged from 0.2 to 0.3° and 0.3 to 0.5°, respectively, and the random error ranged from 0.2 to 0.3° and 0.4 to 0.5°, respectively. Garibaldi reported 0.7–0.9 mm, at 0.4–0.6° of systematic error, and 0.6–0.9 mm, at 0.4° of random error, comparable to the current study [26]. Since SW has no difference in setup accuracy compared to other papers and BF, it is possible to utilize SW for lung SBRT with tumor matching using CBCT. The method of measuring intrafractional setup error used in this study does not capture the real-time motion of a tumor during treatment, and was only representative of the tumor position mid-session.

This study indicated that the wooden baseplate had less effect on the dose distribution than the carbon baseplate because of the lower absorbed dose. In clinical practice, it has been reported that a method to reduce the effect of dose absorption in immobilization systems on dose distribution is to include the immobilization system inside the dose calculation region [33]. However, it is difficult to include the immobilization systems entirely within the FOV because there is a mechanical limit of the CT scanner. In cases where the whole of the immobilization system is not included in the CT image, the effect of the immobilization system on the dose distribution is only partially calculated in the TPS. It is necessary to select immobilization systems that have less effect on the dose distribution.

Conclusion

The wooden baseplate had lower radiation attenuation than the carbon baseplate. The SW, in which the baseplate is made of wood, provided less effect on the dose distribution than the carbon baseplate in SBRT. Compared to conventional systems, the SW is cheaper and required less time for setup, and achieved the same level of setup accuracy as conventional systems.

Acknowledgments

We would like to thank Editage (www.editage.com) for English language editing.

Conflict of interest

None declared.

Funding

Not applicable.

References

1. Fakiris AJ, McGarry RC, Yiannoutsos CT, et al. Stereotactic body radiation therapy for early-stage non-small-cell lung carcinoma: four-year results of a prospective phase II study. Int J Radiat Oncol Biol Phys. 2009; 75(3): 677–682, doi: 10.1016/j.ijrobp.2008.11.042, indexed in Pubmed: 19251380.
2. Hansen AT, Petersen JB, Høyer M. Internal movement, set-up accuracy and margins for stereotactic body radiotherapy using a stereotactic body frame. Acta Oncol. 2006; 45(7): 948–952, doi: 10.1080/02841860600911172, indexed in Pubmed: 16982562.
3. Timmerman R, Papiez L, McGarry R, et al. Extracranial stereotactic radioablation: results of a phase I study in medically inoperable stage I non-small cell lung cancer. Chest. 2003; 124(5): 1946–1955, doi: 10.1378/chest.124.5.1946, indexed in Pubmed: 14605072.
4. Nagata Y, Takayama K, Matsuo Y, et al. Clinical outcomes of a phase I/II study of 48 Gy of stereotactic body radiotherapy in 4 fractions for primary lung cancer using a stereotactic body frame. Int J Radiat Oncol Biol Phys. 2005; 63(5): 1427–1431, doi: 10.1016/j.ijrobp.2005.05.034, indexed in Pubmed: 16169670.
5. Onishi H, Shirato H, Nagata Y, et al. Hypofractionated stereotactic radiotherapy (HypoFXSRT) for stage I non-small cell lung cancer: updated results of 257 patients in a Japanese multi-institutional study. J Thorac Oncol. 2007; 2(7 Suppl 3): S94–100, doi: 10.1097/JTO.0b013e318074de34, indexed in Pubmed: 17603311.
6. Uematsu M, Shioda A, Suda A, et al. Computed tomography-guided frameless stereotactic radiotherapy for stage I non-small cell lung cancer: a 5-year experience. Int J Radiat Oncol Biol Phys. 2001; 51(3): 666–670, doi: 10.1016/s0360-3016(01)01703-5, indexed in Pubmed: 11597807.
7. Fuss M, Salter BJ, Rassiah P, et al. Repositioning accuracy of a commercially available double-vacuum whole body immobilization system for stereotactic body radiation therapy. Technol Cancer Res Treat. 2004; 3(1): 59–67, doi: 10.1177/153303460400300107, indexed in Pubmed: 14750894.
8. Paoletti L, Ceccarelli C, Menichelli C, et al. Special stereotactic radiotherapy techniques: procedures and equipment for treatment simulation and dose delivery. Rep Pract Oncol Radiother. 2022; 27(1): 1–9, doi: 10.5603/RPOR.a2021.0129, indexed in Pubmed: 35402024.
9. Purdie TG, Bissonnette JP, Franks K, et al. Cone-beam computed tomography for on-line image guidance of lung stereotactic radiotherapy: localization, verification, and intrafraction tumor position. Int J Radiat Oncol Biol Phys. 2007; 68(1): 243–252, doi: 10.1016/j.ijrobp.2006.12.022, indexed in Pubmed: 17331671.
10. Grills IS, Hugo G, Kestin LL, et al. Image-guided radiotherapy via daily online cone-beam CT substantially reduces margin requirements for stereotactic lung radiotherapy. Int J Radiat Oncol Biol Phys. 2008; 70(4): 1045–1056, doi: 10.1016/j.ijrobp.2007.07.2352, indexed in Pubmed: 18029110.
11. Guckenberger M, Meyer J, Wilbert J, et al. Precision of image-guided radiotherapy (IGRT) in six degrees of freedom and limitations in clinical practice. Strahlenther Onkol. 2007; 183(6): 307–313, doi: 10.1007/s00066-007-1695-0, indexed in Pubmed: 17520184.
12. Bissonnette JP, Franks KN, Purdie TG, et al. Quantifying interfraction and intrafraction tumor motion in lung stereotactic body radiotherapy using respiration-correlated cone beam computed tomography. Int J Radiat Oncol Biol Phys. 2009; 75(3): 688–695, doi: 10.1016/j.ijrobp.2008.11.066, indexed in Pubmed: 19395200.
13. Li W, Purdie TG, Taremi M, et al. Effect of immobilization and performance status on intrafraction motion for stereotactic lung radiotherapy: analysis of 133 patients. Int J Radiat Oncol Biol Phys. 2011; 81(5): 1568–1575, doi: 10.1016/j.ijrobp.2010.09.035, indexed in Pubmed: 21075559.
14. Zhou J, Uhl B, Dewitt K, et al. Image-guided stereotactic body radiotherapy for lung tumors using BodyLoc with tomotherapy: clinical implementation and set-up accuracy. Med Dosim. 2010; 35(1): 12–18, doi: 10.1016/j.meddos.2008.12.003, indexed in Pubmed: 19931009.
15. Ueda Y, Teshima T, Cárdenes H, et al. Evaluation of initial setup errors of two immobilization devices for lung stereotactic body radiation therapy (SBRT). J Appl Clin Med Phys. 2017; 18(4): 62–68, doi: 10.1002/acm2.12093, indexed in Pubmed: 28503898.
16. Rico M, Martínez E, Pellejero S, et al. Influence of different treatment techniques and clinical factors over the intrafraction variation on lung stereotactic body radiotherapy. Clin Transl Oncol. 2016; 18(10): 1011–1018, doi: 10.1007/s12094-015-1475-8, indexed in Pubmed: 26758718.
17. Han C, Sampath S, Schultheisss TE, et al. Variations of target volume definition and daily target volume localization in stereotactic body radiotherapy for early-stage non-small cell lung cancer patients under abdominal compression. Med Dosim. 2017; 42(2): 116–121, doi: 10.1016/j.meddos.2017.01.008, indexed in Pubmed: 28433482.
18. Olch AJ, Gerig L, Li H, et al. Dosimetric effects caused by couch tops and immobilization devices: report of AAPM Task Group 176. Med Phys. 2014; 41(6): 061501, doi: 10.1118/1.4876299, indexed in Pubmed: 24877795.
19. Chiu-Tsao ST, Chan MF. Evaluation of two-dimensional bolus effect of immobilization/support devices on skin doses: a radiochromic EBT film dosimetry study in phantom. Med Phys. 2010; 37(7): 3611–3620, doi: 10.1118/1.3439586, indexed in Pubmed: 20831069.
20. Vaithianathan H, Harris B. Transmission study of the Abdominal Compression plate (BodyFIX Diaphragm Control) for abdominal and stereotactic body radiotherapy. J Appl Clin Med Phys. 2021; 22(9): 232–241, doi: 10.1002/acm2.13373, indexed in Pubmed: 34339578.
21. Boggs DH, Feigenberg S, Walter R, et al. Stereotactic radiotherapy using tomotherapy for early-stage non-small cell lung carcinoma: analysis of intrafraction tumour motion. J Med Imaging Radiat Oncol. 2014; 58(6): 706–713, doi: 10.1111/1754-9485.12179, indexed in Pubmed: 24767098.
22. Han K, Cheung P, Basran PS, et al. A comparison of two immobilization systems for stereotactic body radiation therapy of lung tumors. Radiother Oncol. 2010; 95(1):

103–108, doi: 10.1016/j.radonc.2010.01.025, indexed in Pubmed: 20189669.
23. Baba F, Shibamoto Y, Tomita N, et al. Stereotactic body radiotherapy for stage I lung cancer and small lung metastasis: evaluation of an immobilization system for suppression of respiratory tumor movement and preliminary results. Radiat Oncol. 2009; 4: 15, doi: 10.1186/1748-717X-4-15, indexed in Pubmed: 19476628.
24. Infusino E. Clinical utility of RapidArc™ radiotherapy technology. Cancer Manag Res. 2015; 7: 345–356, doi: 10.2147/CMAR.S72775, indexed in Pubmed: 26648755.
25. Benkhaled S, Koshariuk O, Van Esch A, et al. Characteristics and dosimetric impact of intrafraction motion during peripheral lung cancer stereotactic radiotherapy: is a second midpoint cone beam computed tomography of added value? Rep Pract Oncol Radiother. 2022; 27(3): 490–499, doi: 10.5603/RPOR.a2022.0040.
26. Mampuya WA, Nakamura M, Matsuo Y, et al. Interfraction variation in lung tumor position with abdominal compression during stereotactic body radiotherapy. Med Phys. 2013; 40(9): 091718, doi: 10.1118/1.4819940, indexed in Pubmed: 24007151.
27. Javadi S, Eckstein J, Ulizio V, et al. Evaluation of the use of abdominal compression of the lung in stereotactic radiation therapy. Med Dosim. 2019; 44(4): 365–369, doi: 10.1016/j.meddos.2019.01.007, indexed in Pubmed: 30852064.
28. Strydhorst JH, Caudrelier JM, Clark BG, et al. Evaluation of a thermoplastic immobilization system for breast and chest wall radiation therapy. Med Dosim. 2011; 36(1): 81–84, doi: 10.1016/j.meddos.2010.01.001, indexed in Pubmed: 20346646.
29. Foster R, Meyer J, Iyengar P, et al. Localization accuracy and immobilization effectiveness of a stereotactic body frame for a variety of treatment sites. Int J Radiat Oncol Biol Phys. 2013; 87(5): 911–916, doi: 10.1016/j.ijrobp.2013.09.020, indexed in Pubmed: 24351410.
30. Garibaldi C, Piperno G, Ferrari A, et al. Translational and rotational localization errors in cone-beam CT based image-guided lung stereotactic radiotherapy. Phys Med. 2016; 32(7): 859–865, doi: 10.1016/j.ejmp.2016.05.055, indexed in Pubmed: 27289354.
31. Korreman SS. Image-guided radiotherapy and motion management in lung cancer. Br J Radiol. 2015; 88(1051): 20150100, doi: 10.1259/bjr.20150100, indexed in Pubmed: 25955231.
32. Josipovic M, Persson GF, Logadottir A, et al. Translational and rotational intra- and inter-fractional errors in patient and target position during a short course of frameless stereotactic body radiotherapy. Acta Oncol. 2012; 51(5): 610–617, doi: 10.3109/0284186X.2011.626448, indexed in Pubmed: 22263924.
33. Park JIn, Ye SJ, Kim HJ, et al. Dosimetric effects of immobilization devices on SABR for lung cancer using VMAT technique. J Appl Clin Med Phys. 2015; 16(1): 5217, doi: 10.1120/jacmp.v16i1.5217, indexed in Pubmed: 25679178.